The 3-D Computational Modeling of Shear-Dominated Ductile Failure in Steel

Franck J. Vernerey, Cahal McVeigh, Wing Kam Liu, Brian Moran, Deepti Tewari, David M. Parks, and Gregory B. Olson

This paper presents recent advances in the computational analysis of the failure mechanisms in high-strength steel. Computational issues are described regarding modeling of the geometry, distribution, and material behavior of the dispersed phases present in the microstructure of steel. The investigation of the failure mechanisms using computational cell model methodology in two and three dimensions is then presented with an emphasis on microvoid-induced shear failure occurring at the scale of submicrometer grain-refining carbide precipitates. The failure of a three-dimensional particle cluster extracted from tomographic analysis of an engineering alloy is simulated. Finally the cell model results are used to simulate the failure of the material at the macro-scale.

INTRODUCTION

The ductility of high-strength steels is often restricted by the onset of a void-sheet mechanism in which failure occurs by a micro-void shear localization process. As part of a "Digital 3-D" consortium effort combining tomographic characterization with three-dimensional (3-D) simulation of realistic microstructures, a micro-void shear instability mechanism is identified here by examining the interactions occurring within a system of multiple embedded secondary particles (carbides, diameter ~10–100 nm) through a finite-element based computational cell modeling technique in two and three dimensions. Shear deformation leads to the nucleation of micro-voids as the secondary particles debond from the surrounding alloy matrix. The nucleated micro-voids grow into elongated void-tails along the principal shear plane and coalesce with the micro-voids nucleated at neighboring particles. The mechanism is incorporated mathematically into a hierarchical model for deformation and failure of steel. The simulated response corresponds to experimentally observed behavior only when the micro-void shear localization mechanism is explicitly considered. The mechanism is explored in further detail through calculations carried out on a cluster of grain-refining carbide particles selected from a model tomographic data set obtained from an IN100 nickel alloy.[1,2]

See the sidebar for details on modeling of the microstructure.

INVESTIGATION OF FRACTURE MECHANISMS

Most of the knowledge regarding fracture mechanisms in steel is a result of observation of fracture surfaces. A typical fracture surface micrograph displays a dimpled structure that gives great insights on the distinct roles of primary and secondary particles. However, this technique gives only a qualitative explanation of the multiple phenomena arising in the failure process and sometimes fails to provide the nature of certain mechanisms, such as in a state of pure shear. This motivates the use of computational mechanics as a tool to investigate mechanisms and to better understand their relations to material microstructures. In this study, computational simulations based on unit-cell models are the primary means by which the micromechanics of the failure process have been investigated.

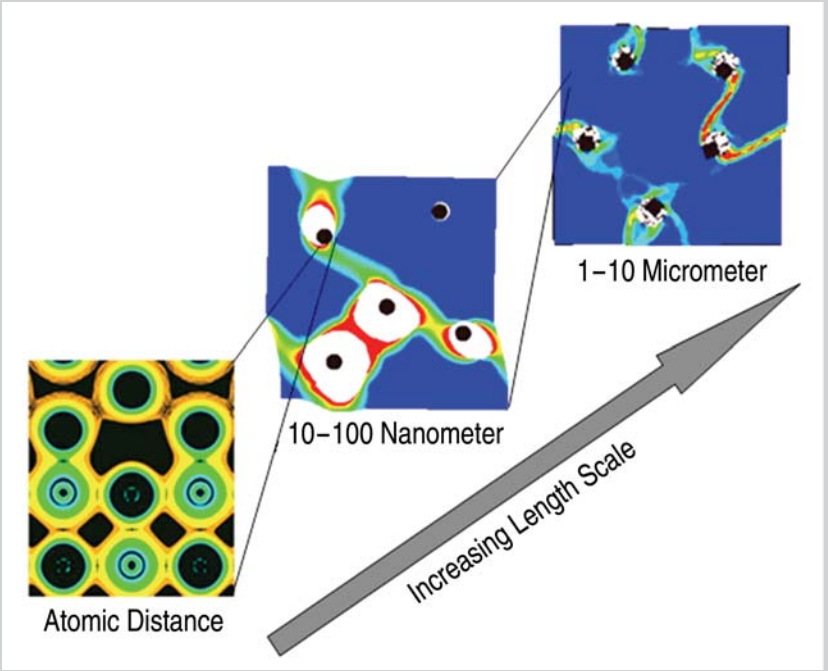

Figure 1. A hierarchical model for high-strength steels, showing three characteristic scales: the atomic scale to assess the debonding of particles, the scale of microvoid-nucleating secondary particles, and the scale of primary void-forming inclusion particles.

Cell Modeling for the Investigation of Ductile Failure Mechanisms

Ductile failure in high-strength steel is a complex process that occurs over different length and time scales. From a modeling viewpoint, it is still impossible to represent all the microstructural features such as dislocations, and primary and secondary inclusions within a single simulation.[14,15] To overcome this constraint, multiscale techniques such as the hierarchical method[11,16] described schematically in Figure 1 are used. In short, this method is a bottom-up approach that consists of homogenizing material properties step by step, from lower to higher scales. At each scale of interest, the microstructure is represented by its own representative volume element, on which various types of loading can be applied. This modeling framework constitutes the platform on which failure mechanisms may be investigated on and across distinct scales.

The definition of a representative volume element (RVE) and the corresponding boundary conditions are known to have significant influence on the average response of the material under investigation.[17] The assumption of a periodic spatial distribution of particles has been widely used in the literature[11,18] as it requires the modeling of only a single particle cell, greatly saving computational cost. This approach gave satisfactory results to explain failure mechanisms in high triaxiality, but, as shown later in this paper, was unable to capture failure mechanisms in pure shear. In this case, the authors believe that only a nonuniform particle distribution could explain the actual physical processes. An important assumption in cell modeling is that the cell must periodically reproduce itself spatially. This assumption is verified if the boundary conditions

MODELING OF THE MICROSTRUCTURE

It is well known that particular microstructural features can have significant effects on the macro-scale deformation and failure properties of materials. In the case of modern high-strength steels, the relevant microstructure can typically be idealized as consisting of three phases: the matrix material, a population of primary inclusion particles at the micrometer scale, and a population of secondary particles (typically grain refining) ranging between tens and hundreds of nanometers. For each of these phases, a large body of experimental data has been gathered, such as, for example, particle size, volume fraction, spatial distribution, and morphology. As each of these features can become critical to the macroscopic properties, an accurate and faithful modeling of the microstructure is necessary.

Microstructure Geometry and Distribution

It is known that the inherent randomness in the distributions of particle size, shape, and spatial locations plays a major role in the ductile failure of alloys and must therefore be accounted for in modeling. For instance, Y. Huang[3] and M.N. Shabrov[4] showed that plastic flow localization depends on the location of particle clusters and the intra-cluster particle average spacing. Hence, in the modeling of high-strength steel, it is of crucial importance to base the computations on a distribution and geometric representation of the critical ductility-limiting microstructural features that are faithful to those of the microstructure. However, an accurate modeling of the microstructural details is often computationally prohibitive. Therefore, in this paper the approach consists of starting with a simplified microstructural description and moving toward more complex and accurate models.

The main failure mechanisms in high-strength steels are generally attributed to the nucleation, growth, and coalescence of voids and microvoids around primary and secondary particles, respectively. As failure often begins at the microstructure's weakest point, clusters of particles are known to be the most likely locations for failure initiation. For this reason, in this study, the modeling of the microstructure is performed for clusters in which the local particle density is higher than the average value found in larger sampling domains.

Material Properties of Phases

In order to capture the essential physics governing the ductile fracture of steel, it is necessary to utilize the best representation possible for the material properties of the various features. A major issue is that at small scales, the behavior of materials and their interactions with other phases may become very complex and require the use of small-scale methods such as molecular dynamics. However, such methods are restricted to relatively small computational domains and therefore cannot be used for domains which comprise one or several secondary particles. Thus, this study mainly remains in the context of continuum mechanics, employing interfacial properties derived from atomistic modeling.

In the present work, two constitutive models were investigated for the matrix material for which the respective uniaxial stress-strain responses are depicted in Figure A The first is represented by a linear hardening J2 flow plasticity, based on experimental behavior of a well-studied high-strength modified 4330 steel.[5] Corresponding material constants are given in Table A. Because the hardening remains constant regardless of the level of strain, this model can be considered an upper bound of the real matrix material behavior when extrapolated to high strains. The second model is based on an internal state variable formulation.[6] Here, a simple isotropic hardening model is used to represent the alloy matrix. The evolution equation for the isotropic hardening strength is motivated from dislocation mechanics, and both dislocation hardening and dynamic recoveries are accounted for. Dislocation hardening refers to dislocation-dislocation impedance. Dynamic recovery may be caused by dislocation cross slip. The yield function is simply stated in Equation 1 (all equations are shown in the Equations table), where $\|\sigma^{dev}\|$ is the tensor norm of the deviatoric Cauchy stress (see Equation 2), κ; initial value $\kappa = 0$ is the isotropic hardening strength; and Y is the initial yield strength. The evolution equation for the isotropic hardening is given by

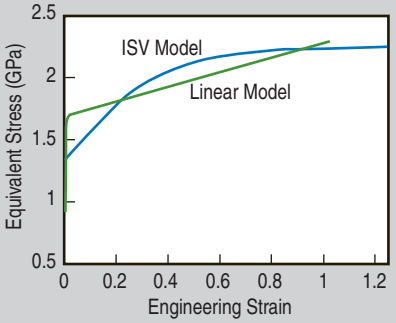

Figure A. A comparison of the tensile stress-strain response of the internal state variable model (ISV) and the linear hardening 4330mod steel model.

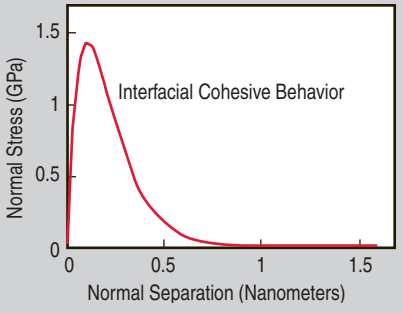

Figure B. A typical force-separation curve at the particle-matrix interface, used at the continuum scale.

Equations

$$\|\sigma^{dev}\| - \kappa - Y = 0 \quad (1)$$

$$\|\sigma^{dev}\| = \sqrt{\frac{3}{2}\sigma_{ij}^{dev}\sigma_{ij}^{dev}} \quad (2)$$

$$\dot{\kappa} = H\sqrt{\frac{2}{3}}\|D^p\| - \left[R_d\sqrt{\frac{2}{3}}\|D^p\|\right]\kappa^2 \quad (3)$$

$$\|D^p\| = \sqrt{\frac{2}{3}D_{ij}^p D_{ij}^p} \quad (4)$$

$$\frac{t}{\hat{t}} = \frac{d}{\hat{d}}\exp\left(1 - \frac{d}{\hat{d}}\right) \quad (5)$$

$$e = \frac{3\gamma}{R} \quad (6)$$

prescribed on the cell surfaces ensure that the displacement profile on two opposite faces of the cell is the same. This gives rise to the so-called periodic boundary conditions that are described in detail in References 12, 17, and 19, and used throughout this paper.

Finally, two types of simulation were used in this study: two-dimensional (2-D) plane strain and fully three-dimensional (3-D) models. The former, even though it approximates particles as circular rods, provides an inexpensive way of investigating potential fracture mechanisms. The latter, more physically representative but also more expensive computationally, can be used to verify that mechanisms observed in simplified 2-D simulations are also valid in three dimensions.

Investigations of Ductile Failure Mechanisms in Two Dimensions

Ductile failure mechanisms in high triaxiality are well documented in the

Equation 3, where H is the hardening modulus, $\|D^p\|$ is the tensor norm of the rate of plastic deformation (see Equation 4), and R_d is the dynamic recovery modulus. This results in a saturation stress being reached where the rate of hardening is equal to the rate of recovery, and the tensor norm of the Cauchy stress deviator remains on a plateau. At the sub-micrometer scale of interparticle matrix ligaments, one can expect scale-dependent effects based on discrete dislocation interactions to play increasingly important roles in local deformation and failure processes, suggesting the desirability of matrix plasticity models based on nonlocal, strain-gradient, or polarized dislocation density flux theories.[7–9] For now, such scale-dependent matrix plasticity models are not considered.

Material models for primary and secondary particles are based on the properties of titanium nitride and titanium carbide, respectively. Nucleation of voids from particles can occur either through cracking of the particles or from decohesion at the particle-matrix interface. In this study, small, strong, equiaxed particles are considered, and therefore cracking is not very likely. Hence, the particles are considered as perfectly elastic, with a high elastic modulus, consistent with experimental data on titanium carbide and titanium nitride. The material constants used in this paper are summarized in Table A, where E denotes the Young's modulus, ν is the Poisson's ratio, H is the hardening modulus, and Y the yield stress.

Finally, the finite-element method was used for material modeling. In this paper, the simulations were performed with the commercial software *ABAQUS/Explicit*©.

Debonding at the Particle-Matrix Interface

The macroscopic fracture of steel often starts with decohesion between particles and the alloy matrix. The interfacial debonding energy and cohesive strength at the iron-carbide interface (Fe-TiC) for secondary particles and iron-nitride (Fe-TiN) for primary particles are therefore major parameters in the fracture process. The determination of the bonding energy between TiC and iron was first performed by Freeman and co-workers[10] using atomic-level first-principles calculations with an all-electron density functional method. Due to the relative sizes of the particles and the atomic spacing, the particle-matrix interface could be approximated by two semi-infinite slabs. In turn, using the periodicity of the assumed atomic structure, the computations were finally based on a primitive periodic cell. The associated energy separation was computed for different atomic arrangements. Because the distance associated with the covalent bond breaking is on the order of the inter-atomic unit, the length scales associated with the debonding expression given by the first-principles calculation are not suitable for resolution at that scale in a continuum mechanics formulation. However, S. Hao et al.[11] showed that the traction-separation relation can be rescaled when considering the effect of dislocations on the interface. Indeed, at the interface, the presence of dislocation cores at empty sites triggers a plastic flow that reduces the decohesion energy significantly. Hao et al. showed that sliding-induced dislocation activity dominates the decohesion process, producing a roughening of the fracture surface and consequently modifying the surface energy and peak stress. This mechanism has the effect of rescaling the traction-separation curve to values for which the separation length scale is resolvable in a continuum mechanics framework. After rescaling, the typical force-separation curve is depicted in Figure B. Following Reference 12, the relationship between the traction t and the separation can be expressed in the convenient non-dimensional form (Equation 5) where $\hat{t}$ is the peak debonding traction and $\hat{d}$ is the separation when $t = \hat{t}$. From the principle of similitude, it can be explained that the larger the inclusion, the earlier the debonding for the same debonding peak force. Indeed, if the surface energy ξ of a particle is given by $\xi = \gamma S$ where γ is the debonding energy per unit surface area and S is the surface area of the inclusion, the debonding energy, e, per unit volume of a spherical inclusion of radius R, is shown in Equation 6.

This quantity decreases as the size of the particle increases, implying that primary particles should debond earlier than secondary. In simulations, the particle-matrix interface conditions written in Equation 5 are modeled with one-dimensional cohesive elements with the "nonlinear spring" option in the software *ABAQUS/Explicit*. This ensures that the traction remains continuous across the interface. More details can be found in Reference 13. In addition, the penalty method was used to model contact between the surfaces of the matrix and the particles.

Table A. Material Constants for 4330mod Steel Linear Model, Internal State Variables Model, and Carbide and Nitride Particles

Model	E_{matrix} (GPA)	ν_{matrix}	Y (GPa)	H (GPa)	R_d	$E_{carbide}$ (GPa)	$\nu_{carbide}$	$E_{nitrice}$ (GPa)	$\nu_{nitride}$
4330mod Steel Linear	210	0.3	1.6	0.56	—	—	—	—	—
Internal State Variables	210	0.3	1.6	5.6	2e-8	—	—	—	—
Carbide and Nitride Particles	—	—	—	—	—	630	0.3	630	0.3

literature.[6,20] Generally, three main stages can be observed: nucleation of cavities from primary particles, void growth, and failure of the material by a microvoid sheet nucleated from secondary particles. The formation of a microvoid sheet corresponds to the nucleation, growth, and coalescence of microvoids at the site of secondary particles. Figure 2 shows the evolution of equivalent plastic strain from a simulation in which two cuboidal primary particles (TiN) are modeled explicitly, and (effects of) secondary particles are modeled through a homogenized damage model accounting for nucleation, growth, and coalescence of microvoids. The last frame depicts the formation of a microvoid sheet at 45 degrees that is triggered by the interaction between the voids nucleated from the primary particles and microvoids nucleated from secondary particles.

The precise nature of ductile fracture mechanisms in low triaxiality is still debated within the material science community. Experimental evidence[21] shows that failure in shear strongly depends on the population of secondary particles. However, shear failure on the scale of dispersed grain-refining carbides is not well understood. Therefore, numerical simulations are used based on unit cell-calculations as a tool to investigate these mechanisms. The first attempt was made in the context of a uniform periodic particle distribution using the unit cell depicted in Figure 3. After discretizing the cell with finite elements, one prescribes the cell to a state of pure shear strain (but zero net stress perpendicular to the shear plane) using periodic boundary conditions. In this example, the matrix material is linearly hardening and the volume fraction of the particle is 4%, well in excess of ~1%, the latter being a typical overall average volume fraction of such carbides (~0.5%). Figure 3 shows the effects of particle-matrix interface peak cohesive strength on the overall response of the cell. Three observations can be made. First, the debonding of the particle triggers a steep softening in the stress-strain curve, but in this ideally dispersed microstructure the material recovers afterward. Second, the average debonding strain increases with the norm of the debonding peak stress, and third, after debonding, the material response converges with the response of the material with no bonding between the particles and the matrix. Therefore, although a softening event is observed during particle-matrix debonding, the resulting "transient" instability is confined to the local debonding event and thereafter the stress-strain curve continues to harden. In other words, no failure localization mechanisms could be obtained with this simplified particle configuration.

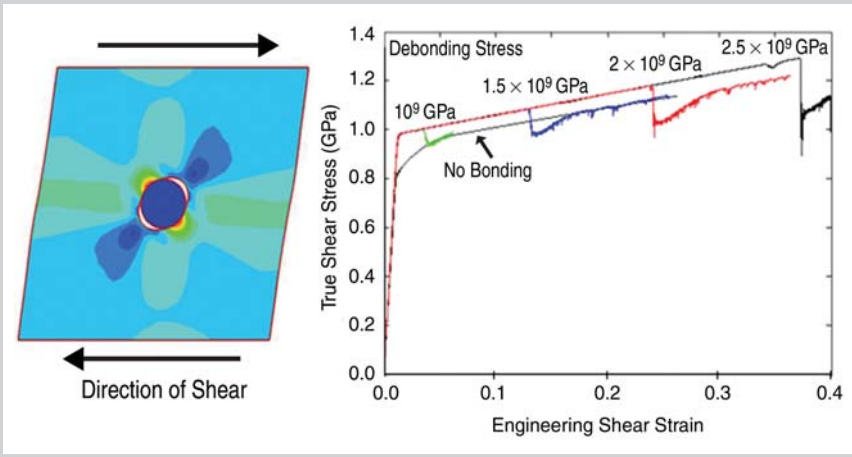

Figure 3. Plastic strains in a 2-D plane-strain periodic unit cell subject to pure shear and average cell response for different debonding peak stress.

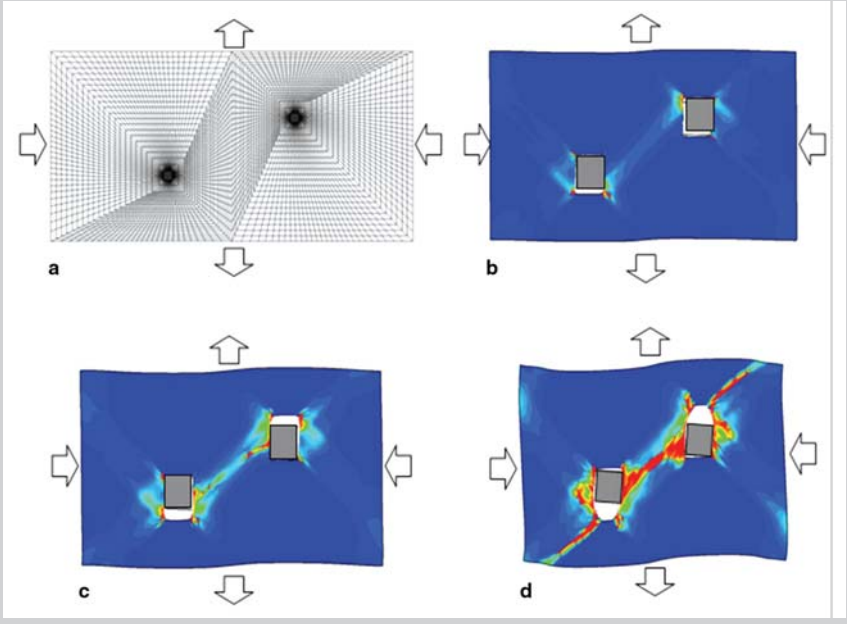

Figure 2. (a) Finite-element mesh and (b, c, d) contours of plastic strain showing the void sheet mechanism between two voids nucleated from cuboidal primary particles.

The effect of particle distribution was then investigated by simulating the shear deformation of a cluster of nine secondary particles with RVE volume fraction 2% and particle radii in the range 30–50 nm, as shown in Figure 4. In this computation, the matrix properties correspond to the 4330mod steel linear model (Table A). The average response of the cell is displayed in Figure 4. It is seen to exhibit a softening behavior due to material failure. This result accentuates the role of particle distribution on the failure of high-strength steel. The failure mechanism can be explained as a result of microvoid coalescence in a plane whose direction coincides with the shearing direction. After observation of Figure 4, one can note that in this plane, the top of one particle is aligned with the bottom of another. Upon loading, the embedded particles debond from the surrounding

matrix and as they are driven toward each other, the nucleated microvoids begin to grow along the evolving plane of shear localization. The tail-like elongated microvoids propagate toward each other, in a similar manner to the propagation of a shear crack. Eventually, the ligament between the voids undergoes instability through necking. As deformation increases, the particles are also driven toward each other, increasing the severity of the coalescence. As a result, the macroscopic stress-strain curve displays severe "terminal" softening after coalescence has occurred. This mechanism is investigated in detail in Reference 13.

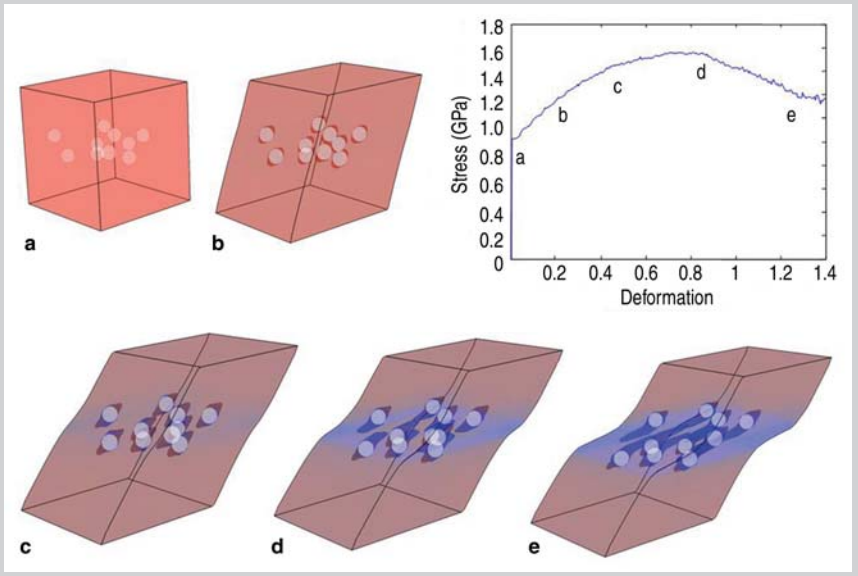

Figure 5. The evolution of equivalent plastic strain in a 3-D particle cluster model and corresponding average response of the cell under applied shear.

Failure Mechanisms in Three Dimensions

After identification of the potential shear failure mechanism at the scale of secondary particles in 2-D, a 3-D analysis is performed. The 3-D analysis is not only necessary to validate the 2-D results, but it is also essential for obtaining more realistic quantitative results that can ultimately be used for materials design.

Several 3-D clusters were modeled with different particle densities and distributions. Both material models presented previously were used to model the matrix material, and periodic boundary conditions were used. Several key observations can be made. First, in order to obtain the failure mechanism described, the local particle fraction within the RVE must be higher in 3-D simulations than in the equivalent 2-D model. This can be explained by the fact that spheres are not as prone to interact via localized matrix shearing as are cylinders under plane strain. Second, 3-D shear failures were not obtained with the linear hardening matrix material. However, the ISV model gave satisfactory results. Indeed, because it exhibits a saturation point, the ISV model promotes localization of the deformation in the necking region between neighboring voids as large strains are reached. Finally, the average response of the cell is similar to the 2-D equivalent model. A softening behavior is observed when neighboring microvoids start coalescing. Figure 5 shows the evolution of plastic strain for a 3-D cluster that is located in a horizontal plane. Microvoid tails and coalescence can be observed. The corresponding shear stress-strain response is displayed along with the location of each frame on this curve.

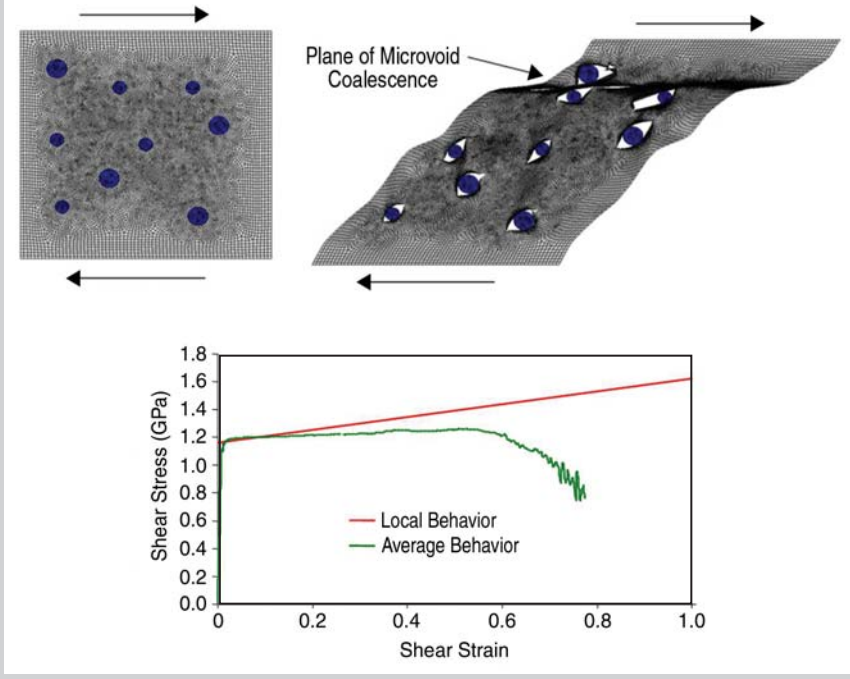

Figure 4. The shear deformation of a 2-D plane-strain particle cluster. Periodic boundary conditions are used. Failure concentrates in a plane are determined by the placement of particles. The average behavior is given for the cell and for the matrix material for comparison.

Failure Mechanisms in a Real Microstructure

A statistical study of the particle distribution, size, and spacing was performed based on a grain-refining carbide data set obtained from tomographic characterization of a nickel alloy.[1,2] In view of the similar grain sizes and overall volume fraction of grain-refining carbides in this alloy and in representative high-strength steels, we are using the IN100 carbide data as a 3-D model microstructure. A volume of approximately 30 μm^3 was serially sectioned using focused-ion-beam technology,[1]

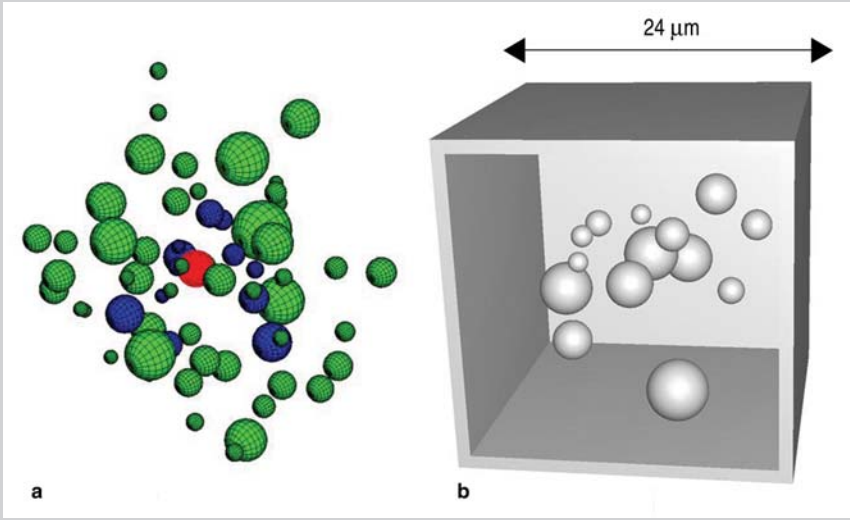

Figure 6. (a) An illustration of the chosen IN100 particle cluster, including scaled particle diameters. The cluster centers on the red particle; its Vornoi neighbors are the blue particles. In turn, the green particles comprise the set of next nearest neighbors. (b) The geometry of the computational unit cell of the cluster of central and nearest neighbor particles.

and the resulting compositional data set was discretized[2] into a set of ~12,000 carbide centroids and equivalent diameters. Voronoi tesselation of the centroids yielded 9,080 particles with complete nearest-neighbor tesselations, comprising an average particle volume fraction of 1.7%. In turn, the topology of the tesselation provided the complete set of nearest neighbors, locations and diameters, and associated statistics. The average number of particle neighbors ranged from 6 to 33, with a mean value of 15. The authors selected a cluster of particles in which failure was deemed likely to start (i.e., it combines larger particle size and smaller inter-particle distances). The chosen cluster consists of 14 particles whose local volume fraction is 4.7%, and is represented by the red and blue particles in Figure 6a. In order to analyze the mechanical response of the cluster, a cubic computational cell model (using the finite-element method) is constructed as shown in Figure 6b.

The finite-element discretization consists of hexahedral eight-node brick elements, and periodic boundary conditions are applied. The constitutive behavior of the matrix material is given by the internal state variable model. The contours of plastic strains and the average response of the cell can be seen in Figure 7. Failure of the cell (onset of softening) is observed at about 120% strain. This result indicates that the cluster is a favorable location for the beginning of a failure in the material. The accumulated damage can then propagate to another nearby cluster and form a crack.

Effect of Microvoid Shear Softening on the Macroscopic Behavior

In order to understand and quantify the consequences of the microscopic failure mechanisms on the overall behavior of high-strength steel, it is important to incorporate them into a continuum-based constitutive relation. Thus, modifications are made to phenomenological constitutive models (such as the Gurson model[18]) in order to capture some of the features associated with microvoiding, including the rapid loss of stress-carrying capacity of the material in pure shear. One of the most-used constitutive models for the failure of alloys, the Gurson model, is based on the nucleation, growth, and coalescence in a state of high triaxiality. Consequently, this model is incapable of describing the failure of the material when there is no volumetric strain. In this study, therefore, the form of the model was modified to include the effects of microvoid coalescence in pure shear, such as described previously. Details of the formulation can be found in Reference 13.

The improved model was used to reproduce a ballistic experimental result of a bullet impacting a steel shell. Ballistic tests on high-strength steel shells typically exhibit plugging phenomena.[21] In other words, the impact of the bullet on the shell triggers the formation of bands of intense shear that promote the failure of the material under pure shear conditions. The problem is simulated in plane-strain conditions using both the conventional Gurson model[13] and the improved damage model for comparison. Figure 8 provides a comparison of the profile of plastic strain for both cases. The left figure represents the profile of

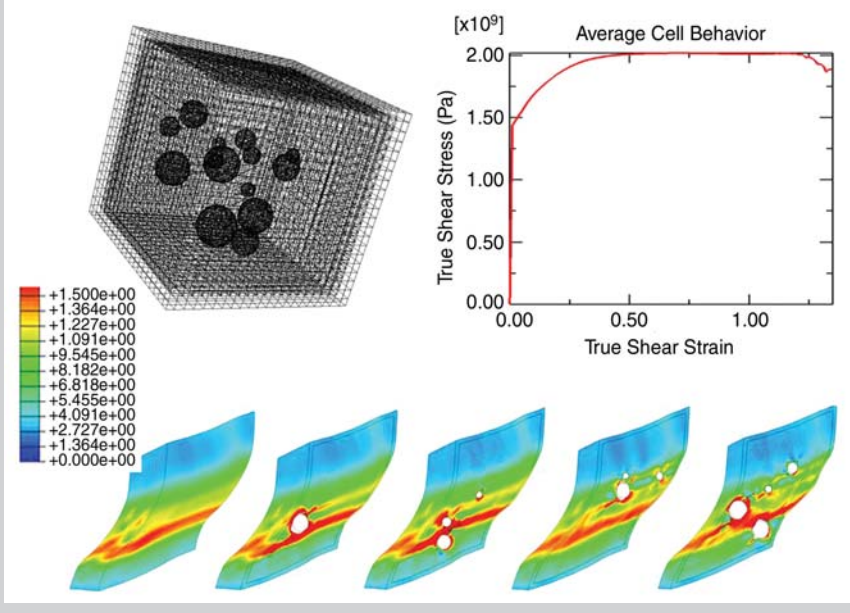

Figure 7. Finite-element mesh and corresponding contours of plastic strain subjected to pure shear strain and overall stress-strain response. The plastic strains are shown on the surface of the cell with the elements and across several sections of the cell.

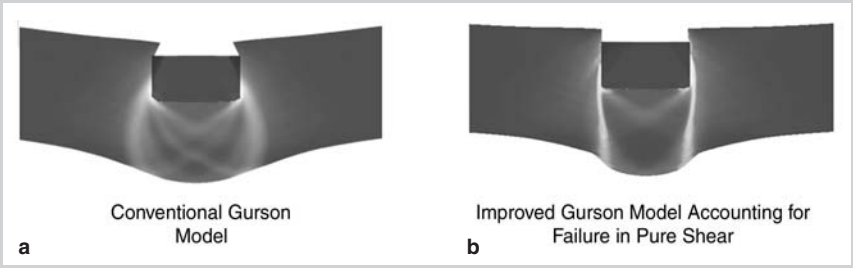

Figure 8. The contours of equivalent plastic strain are plotted for the solution given by (a) the conventional Gurson model and (b) for the improved Gurson, accounting for the microvoid softening failure mechanisms in pure shear. The improved model displays the plugging effect observed experimentally.[21]

the shell after impact and the corresponding contours of plastic strain when the conventional Gurson model is used. In this case, due to the very low hydrostatic stress, the Gurson model predicts little void growth and therefore no ductile failure. Consequently, the impact triggers bending of the shell, but no plugging effect is observed. Figure 8b represents the profile of the shell after impact and the corresponding contours of plastic strain when the modified Gurson model is used. Because of its ability to handle failure in pure shear, the localization of the plastic deformation into two sharp shear bands (or microvoid sheets) is observed on each side of the bullet, with very little bending of the shell. The failure of the material in these shear bands subsequently allows a piece of material to pop out beneath the shell, as observed in ballistic experiments.[21] The modified model therefore reproduces well the plugging phenomena.

CONCLUSION

The use of finite elements as a tool to investigate the failure mechanisms of high-strength steel has been demonstrated. Moving from simplified 2-D computations to the simulation of a real particle cluster in three dimensions was useful to determine a priori the essential physics of the failure mechanism. The real cluster simulation gave satisfactory results and opens new possibilities for quantifying the effects of key microstructural features such as particle-matrix bonding strength and particle density on the toughness and shear localization resistance of steel. To study the failure of steel across several scales of microstructure, the 3-D simulations of a real microstructure presented in this paper can ultimately be used together with multi-scale methods such as those introduced in References 15, 16, 22. To overcome the limitations of the finite-element methods in cases of large deformation, alternative meshless computational methods[23] can also be used.

ACKNOWLEDGEMENTS

The authors gratefully acknowledge the support of the Office of Naval Research D3D Digital Structure Consortium (award N00014-05-C-0241) and the National Science Foundation.

References

1. M. Uchic, Air Force Research Laboratory, unpublished research.
2. H.-J. Jou, Ques Tek Innovations LLC, unpublished research.
3. Y. Huang, "The Role of Nonuniform Particle Distribution in Plastic Flow Localization," *Mechanics of Materials,* 16 (1993), pp. 265–279.
4. M.N. Shabrov and A. Needleman, "An Analysis of Inclusion Morphology Effects on Voids Nucleation," *Modeling and Simulation in Materials Science and Engineering,* 10 (2) (March 2002), pp. 163–183.
5. M. Shabrov et al., "Void Nucleation by Inclusion Cracking," *Metall. and Mater. Trans. A,* 35A (2004), p. 1745.
6. M.F. Horstemeyer et al., "Modeling Stress State Dependent Damage Evolution in a Cast Al-Si-Mg Aluminium Alloy," *Theoretical and Applied Fracture Mechanics,* 33 (2000), pp. 31–47.
7. M.F. Ashby, "The Deformation of Plastically Non-Homogeneous Alloys," *Philos. Mag.,* 21 (1970), pp. 399–424.
8. A. Arsenlis et al., "On the Evolution of Crystallographic Dislocation Density in Nonhomogeneously Deforming Crystals," *J. Mech. Phys. Solids,* 52 (2004), pp. 1213–1246.
9. H. Gao et al., "Mechanism-Based Strain Gradient Plasticity—I. Theory," *J. Mech. Phys. Solids,* 47 (1999), pp. 1239–1263.
10. A.J. Freeman, "Materials by Design and the Exciting Role of Quantum Computation/Simulation," *J. Computational and Applied Mathematics,* 149 (1) (2002), pp. 27–56.
11. S. Hao et al., "Multiple-Scale Constitutive Model and Computational Framework for the Design of Ultra-High Strength, High Toughness Steels," *Comput. Methods Appl. Mech. Engrg.,* 193 (2004), p. 1865.
12. F.J. Vernerey, W.K. Liu, and B. Moran, "Multi-Scale Continuum Theory for Microstructured Materials," submitted to the *Journal of the Mechanics and Physics of Solids.*
13. C. McVeigh et al., "An Interactive Microvoid Localization Mechanism in High Strength Steels," *J. Mech. Phys. Solids,* in press.
14. W.K. Liu et al., "An Introduction to Computational Nanomechanics and Materials," *Comput. Methods Appl. Mech. Engrg.,* 193 (2004), pp. 1529–1578.
15. W.K. Liu, E.G. Karpov, and H.S. Park, *Nano Mechanics and Materials, Theory, Multiscale Methods and Applications* (New York: Wiley, 2006).
16. F.J. Vernerey, "Multi-scale Continuum Theory for Microstructured Materials" (Ph.D. thesis, Northwestern University, 2006).
17. V. Kouznetsova, "Computational Homogenization for the Multi-Scale Analysis of Multi-Phase Materials" (Ph.D. thesis, Technische Universiteit Eindhoven, 2002).
18. A.L. Gurson, "Continuum Theory of Ductile Rupture by Void Nucleation and Growth: Part 1. Yield Criteria and Flow Rules for Porous Ductile Media," *ASME J. Engrg. Mater. Technol.,* 99 (1977), pp. 2–15.
19. M. Danielsson, D.M. Parks, and M.C. Boyce, "Three-Dimensional Micromechanical Modeling of Voided Polymeric Materials," *J. Mech. Phys. Solids,* 50 (2002), pp. 351–379.
20. P.F. Thomason, *Ductile Fracture of Metals* (Oxford, U.K.: Pergamon Press, 1990).
21. J.G. Cowie, M. Azrin, and G.B. Olson, "Microvoid Formation during Shear Deformation of Ultrahigh Strength Steels," *Metallurgical Transactions,* 20A (1989), pp. 143–153.
22. C. McVeigh et al., "Multiresolution Analysis for Material Design," *Comput. Methods Appl. Mech. Engrg.,* 195 (2006), pp. 5053–5076.
23. W.K. Liu, S. Jun, and Y.F. Zhang, "Reproducing Kernel Particle Methods," *Int. J. Numerical Methods in Fluids,* 20 (1995), pp. 1081–1106.

Franck J. Vernerey and Brian Moran are with the Department of Civil and Environmental Engineering; Cahal McVeigh and Wing Kam Liu are with the Department of Mechanical Engineering; and Gregory B. Olson is with the Department of Materials Science, all at Northwestern University in Evanston, Illinois. Deepti Tewari and David M. Parks are with the Department of Mechanical Engineering at the Massachusetts Institute of Technology in Cambridge, Massachusetts.

For more information, contact Gregory B. Olson, Northwestern University, Department of Mechanical Engineering, 2145 Sheridan Road, Evanston, IL, 60208-3111, USA; (847) 491-2847; fax (847) 491-7820; e-mail g-olson@northwestern.edu.